15

Different-Strength Singularities

This chapter deals with phase shift functions that have two sets of singularities, being of different degrees. The "Fermi" phase shift function

$$X(b_x) = \frac{A_{\mathrm{F}}}{1 + \exp[(b_x - c)/\beta]}, \quad \mathrm{Re}\, b_x > 0, \tag{15.1}$$

will play a central role in this discussion, as a common reference. Its derivative, $X'(b_x)$ has pole singularities of second order, at $b_x = \mp c - i\pi\beta$. At large momentum transfers, the points of stationary phase will be attracted to these singularities. However, if the derivative of the overall phase shift function has a more singular point nearby, such a point may exert a stronger attraction on the stationary points. In this way, as the momentum transfer increases, the stationary points may move past those singularities associated with the ordinary "Fermi" distribution, towards other and stronger singularities. We shall in the following sections discuss a few such examples.

In this discussion, maps of the impact parameter plane are very useful for showing possible locations of points of stationary phase. In particular, the maps show where points of stationary phase are located with respect to the singularities of the phase shift function, to which they may asymptotically get attracted at large momentum transfers.

First, in Sections 15.1 and 15.2 we will consider combinations of "Fermi" functions to different (finite) powers,

$$X(b_x) = \frac{A_{\mathrm{F}1}}{1 + \exp[(b_x - c_1)/\beta_1]} + \frac{A_{\mathrm{F}2}}{\{1 + \exp[(b_x - c_2)/\beta_2]\}^p}, \quad \mathrm{Re}\, b_x > 0,$$
$$X(-b_x) = X(b_x), \tag{15.2}$$

with $p \neq 1$. If $p > 1$, the contribution to $X'(b_x)$ originating from the second term will be more singular, and thus exert a stronger attraction on the trajectory of

Downloaded from https://www.cambridge.org/core. UNIVERSIDAD AUTONOMA METROPOLITANA, on 16 Nov 2026 at 02:58:46, subject to the Cambridge Core terms of use, available at https://www.cambridge.org/core/terms. https://doi.org/10.1017/9781316219256.019

stationary points. On the other hand, if $p < 1$, it will be less singular, and exert a weaker attraction. Below, we study two cases, $p = 2$ (squared "Fermi" distribution) and $p = 1/2$ (square root of "Fermi" distribution).

Then, in Section 15.3 we will consider the combination of a "Fermi" distribution, which yields a second-order singularity, together with a Gaussian one, which yields an *essential* singularity (at $(\mathrm{Re}\, b_x, \mathrm{Im}\, b_x) = (0, -i\infty)$).

We are here trying to find a function that for some range of momentum transfers leads to quasi-stable oscillations with a certain "envelope" or overall decrease of the maxima of the oscillations, but where they eventually change to a longer period and a steeper "envelope." In terms of analytic properties, we are looking for functions which have two sets of singularities. These should be located such that at moderate momentum transfers the trajectories of stationary points are attracted to the outer set (larger $|\mathrm{Re}\, b_x|$), but then at larger momentum transfers they would get more attracted to an inner set (smaller $|\mathrm{Re}\, b_x|$). For these functions to have the desired properties, the inner singularity should be stronger. Clearly, also the relative strengths $A_{\mathrm{F}1}$ and $A_{\mathrm{F}2}$ will be important.

15.1 "Fermi" and Squared "Fermi" Functions

We consider first

$$X(b_x) = \frac{A_{\mathrm{F}1}}{1 + \exp[(b_x - c_1)/\beta_1]} + \frac{A_{\mathrm{F}2}}{\{1 + \exp[(b_x - c_2)/\beta_2]\}^2}, \quad \mathrm{Re}\, b_x > 0,$$
$$X(-b_x) = X(b_x), \tag{15.3}$$

i.e., a "Fermi" function plus the square of another one. While the derivative of the first term has a pole singularity of second order, the second term will yield a singularity of the third order.

It is instructive to first understand scattering from the squared "Fermi" function in isolation, i.e., the case $A_{\mathrm{F}1} = 0$. A very important constraint on the location of stationary points is that $X'(b_x)$ should be real. We recall that in the neighborhood of the second-order poles of the derivative of the "Fermi" phase shift function, there are four directions in the complex b_x-plane, along which $X'(b_x)$ is real. (It is positive along every second one of these "rays".) The derivative of the squared "Fermi" function has poles of *third* order, and thus there are altogether six directions along which $X'(b_x)$ is real. It is positive along three of them.

We show in Fig. 15.1 the map of possible positions of stationary points in the complex b_x-plane, for the parameters

$$A_{\mathrm{F}} = i, \quad (c, \beta) = (3.0, 0.5)\ \mathrm{fm}. \tag{15.4}$$

Downloaded from https://www.cambridge.org/core. UNIVERSIDAD AUTONOMA METROPOLITANA, on 16 Nov 2026 at 02:58:46, subject to the Cambridge Core terms of use, available at https://www.cambridge.org/core/terms. https://doi.org/10.1017/9781316219256.019

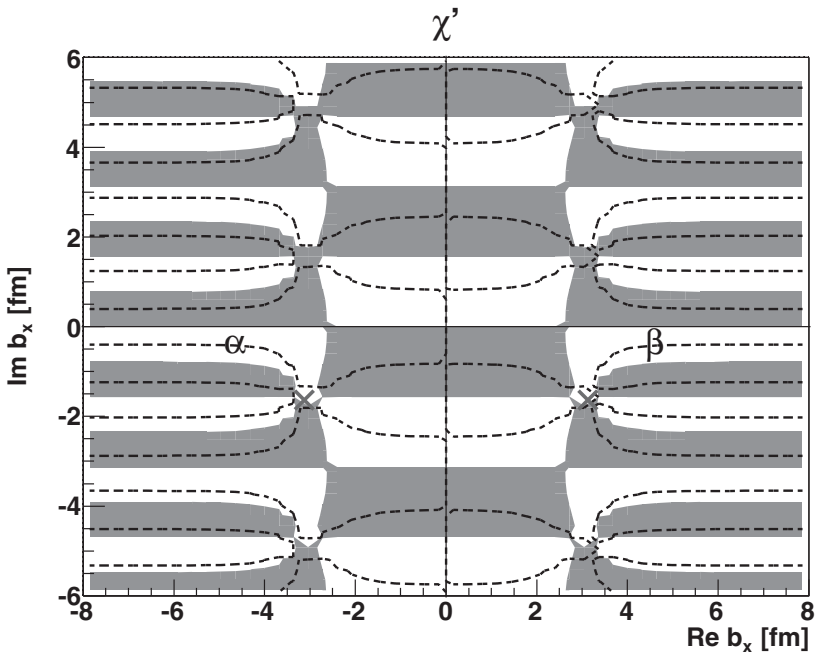


Figure 15.1 Regions of positive and negative values of $\mathrm{Re}\, X'(b_x)$, shown in the complex b_x-plane for only the quadratic part of the phase shift function Eq. (15.3), i.e., with $A_{\mathrm{F1}} = 0$. The dashed curves indicate where $\mathrm{Im}\, X'(b_x) = 0$, i.e., where stationary points may be located. The crosses indicate relevant singularities of the phase shift function. The shape parameters are $(c_2, \beta_2) = (3, 0.5)$ fm.

The relevant singularities are indicated by crosses, and the segments of lines where $X'(b_x)$ is both real and positive, and also closest to the real axis, are denoted α and β.

We recall from Chapter 10 that the angle of approach to the singularity is given by the degree of the singularity, and indeed, the trajectories approach the singularities at an angle of $-\pi/2$, steeper than for the ordinary "Fermi" phase shift function, discussed in Chapter 8, where the corresponding angles of approach are $\pm\pi/4$. This means that in the "final approach," the period of oscillation will be absolutely stable, whereas there will be some steepening of the overall slope.

In Fig. 15.2 we compare the resulting differential cross section (solid) with that corresponding to the ordinary "Fermi" phase shift function (dashed). The squared "Fermi" phase shift function is seen to produce a less steeply falling cross section (with stationary points closer to the real axis), and at small momentum transfers displays some lengthening of the period of oscillation. These features are consistent with the fact that the stationary points approach the singularity at a different angle, compared to the case of the ordinary "Fermi" function. Furthermore, the less steep

Downloaded from https://www.cambridge.org/core. UNIVERSIDAD AUTONOMA METROPOLITANA, on 16 Nov 2026 at 02:58:46, subject to the Cambridge Core terms of use , available at https://www.cambridge.org/core/terms. https://doi.org/10.1017/9781316219256.019

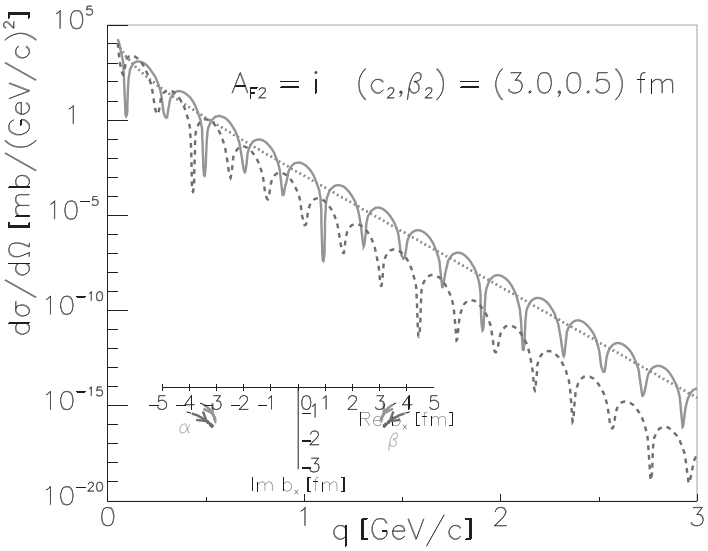


Figure 15.2 Solid: Differential cross sections corresponding to the phase shift function Eq. (15.3) with parameters corresponding to Eq. (15.4) and $A_{F1} = 0$. The inserts show the trajectories of stationary points for $0.02\,\text{GeV/c} \leq q \leq 5.0\,\text{GeV/c}$ (dotted). Heavy dashed: The corresponding differential cross section for the "Fermi" phase shift function, with the same shape parameters.

envelope associated with the sharper edge reflects the fact that the effective surface thickness is $\beta_2/2$. This behavior is also reminiscent of the fact that for the limit of a black disk the differential cross section is given by the square of a Bessel function, without any exponential damping at all. Again, the asymptotic approximation agrees well with the direct numerical evaluation of the diffraction integral (not shown).

Let us now allow both terms in Eq. (15.3) to simultaneously be present. If these two singularities are suitably located with respect to each other, the stationary points may initially (for small and moderate values of momentum transfer) approach the outer and weaker ones, at $\mp c_1 - i\pi\beta_1$, but then at larger momentum transfers bypass these and move towards the other set, at $\mp c_2 - i\pi\beta_2$. However, this does not happen automatically, only for certain ranges of the parameters.

We show in Fig. 15.3 the map of possible positions of stationary points in the complex b_x-plane, for the parameters

$$\begin{aligned} A_{F1} &= i, \quad (c_1,\beta_1) = (4.0,0.5)\ \text{fm}, \\ A_{F2} &= i, \quad (c_2,\beta_2) = (1.5,1.0)\ \text{fm}. \end{aligned} \tag{15.5}$$

The relevant singularities are indicated by crosses, and the segments of lines where $X'(b_x)$ is both real and positive, and also closest to the real axis, are denoted α, α', β, and β'.

Downloaded from https://www.cambridge.org/core. UNIVERSIDAD AUTONOMA METROPOLITANA, on 16 Nov 2026 at 02:58:46, subject to the Cambridge Core terms of use, available at https://www.cambridge.org/core/terms. https://doi.org/10.1017/9781316219256.019

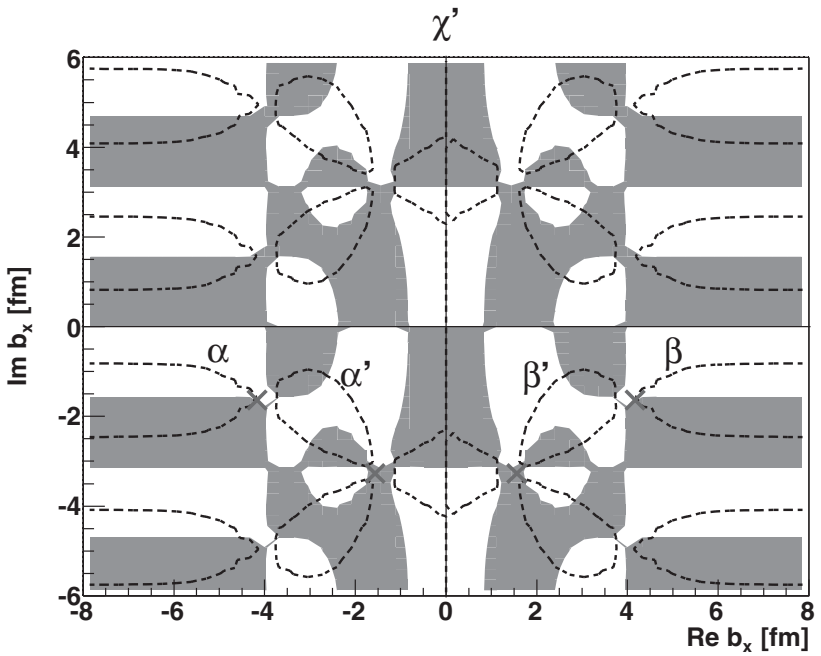


Figure 15.3 Regions of positive and negative values of $\mathrm{Re}\, X'(b_x)$, shown in the complex b_x-plane for the phase shift function Eq. (15.3). The dashed curves indicate where $\mathrm{Im}\, X'(b_x) = 0$, i.e., where stationary points may be located. The crosses indicate singularities of the phase shift function. The shape parameters are $(c_1, \beta_1) = (4, 0.5)$ fm, with $A_{\mathrm{F}1} = i$, and $(c_2, \beta_2) = (1.5, 1.0)$ fm, with $A_{\mathrm{F}2} = i$.

Away from the singularities, and the line $\mathrm{Re}\, b_x = 0$, the function $X'(b_x)$ is analytic. Hence these (dashed) lines are continuous, and do not intersect (this fact is not fully demonstrated by the available resolution).

If we gradually increase the strength associated with the more singular part of the phase shift function, i.e., make $A_{\mathrm{F}2}/A_{\mathrm{F}1}$ larger, then the shaded region (where $\mathrm{Re}\, X'(b_x) < 0$) separating them will shrink, but the two branches α and α' (as well as β and β') remain disconnected up to $A_{\mathrm{F}2}/A_{\mathrm{F}1} = \mathcal{O}(200)$. Somewhere in that range, however, they merge.

One can also make these curves move around in the complex b_x-plane by changing the shape parameters. As an illustration of this, we take the two singularities to be closer to each other, with

$$\begin{aligned} A_{\mathrm{F}1} &= i, \qquad (c_1, \beta_1) = (3, 0.5)\ \text{fm}, \\ A_{\mathrm{F}2} &= 10i, \quad (c_2, \beta_2) = (2.5, 0.75)\ \text{fm}, \end{aligned} \tag{15.6}$$

and show in Fig. 15.4 the "map" of possible trajectories of stationary points in the complex b_x-plane. The relevant singularities are again marked as crosses. The

Downloaded from https://www.cambridge.org/core. UNIVERSIDAD AUTONOMA METROPOLITANA, on 16 Nov 2026 at 02:58:46, subject to the Cambridge Core terms of use , available at https://www.cambridge.org/core/terms. https://doi.org/10.1017/9781316219256.019

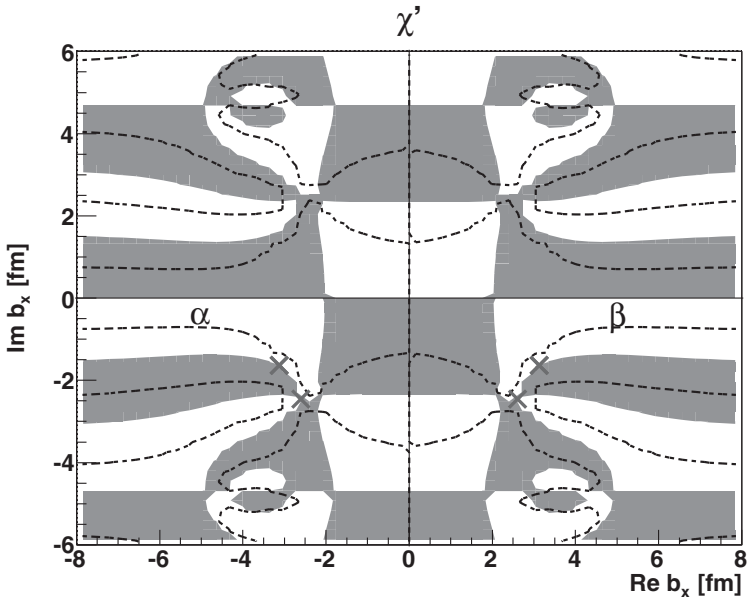


Figure 15.4 Similar to Fig. 15.3, for shape parameters $(c_1, \beta_1) = (3, 0.5)$ fm, $(c_2, \beta_2) = (2.5, 0.75)$ fm, and $A_{\mathrm{F}2} = 10i$.

dashed lines labeled α and β are now seen to stay in the white region (where $X'(b_x) > 0$) and circumvent the outer set of singularities by passing *above*, i.e., closer to the real axis.

If we now gradually increase the value of c_2, at some point around 2.8–2.9 fm, the trajectory flips to the other side, i.e., it passes *below* the outer singularity, as illustrated in Fig. 15.5.

When it comes to constructing the differential cross section, it is important to keep in mind that this "map" is invariant if we keep the (c_i, β_i) fixed, but scale the strengths, $A_{\mathrm{F}1}$ and $A_{\mathrm{F}2}$, as long as the ratio $A_{\mathrm{F}2}/A_{\mathrm{F}1}$ is kept fixed. Such a scaling will just amount to a scaling of the momentum transfer that corresponds to a certain point on the (dashed) curve. However, while the positions of the stationary points are essential for the dependence of the differential cross section on the momentum transfer, they are not the whole story. Also the absolute value of $X(b_x)$ is relevant, and this is affected by the choices of $A_{\mathrm{F}1}$ and $A_{\mathrm{F}2}$.

In Fig. 15.6 we show the differential cross section corresponding to the phase shift function Eq. (15.3) for the parameters adopted in Fig. 15.5, except that we have scaled down the overall strength by a factor of 10, i.e., we have taken $A_{\mathrm{F}1} = 0.1i$ and $A_{\mathrm{F}2} = i$. As anticipated from the discussion above, the additional and stronger singularities further away from the real axis make the envelope of the differential cross section fall in a steeper fashion.

Downloaded from https://www.cambridge.org/core. UNIVERSIDAD AUTONOMA METROPOLITANA, on 16 Nov 2026 at 02:58:46, subject to the Cambridge Core terms of use , available at https://www.cambridge.org/core/terms. https://doi.org/10.1017/9781316219256.019

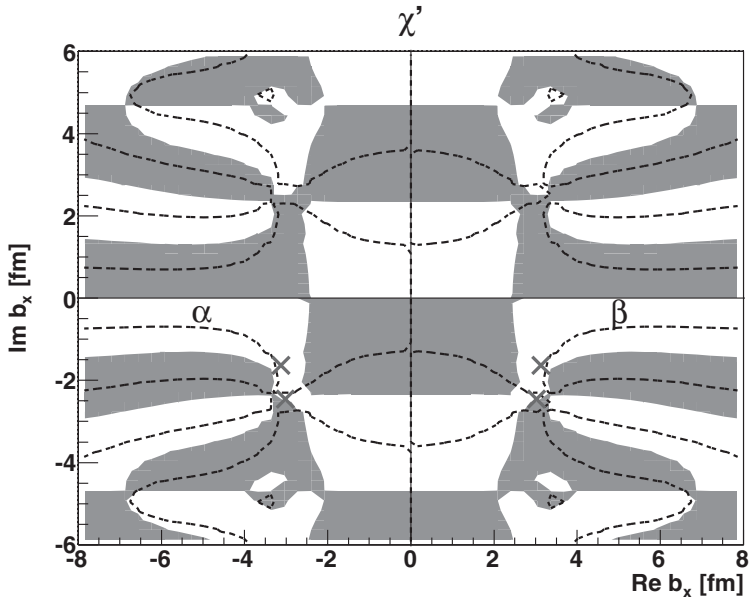


Figure 15.5 Similar to Fig. 15.4, for the phase shift function Eq. (15.3). The shape parameters are $(c_1, \beta_1) = (3, 0.5)$ fm, $(c_2, \beta_2) = (2.9, 0.75)$ fm, with $A_{F2} = 10i$.

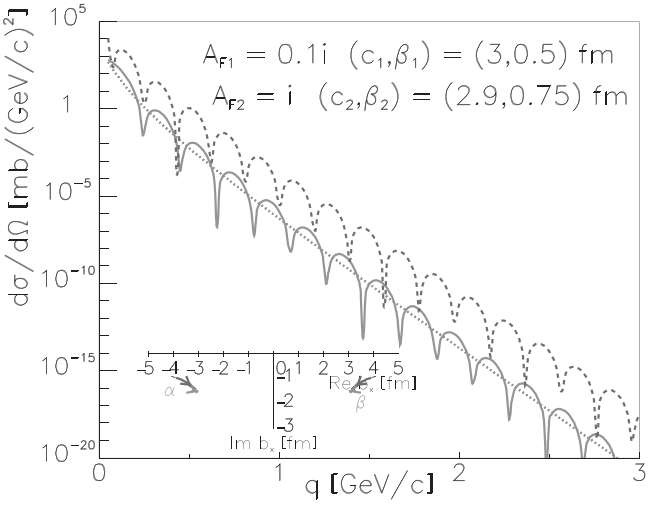


Figure 15.6 Solid: Differential cross sections corresponding to the phase shift function Eq. (15.3). The inserts show the trajectories of stationary points for 0.02 GeV/c $\leq q \leq$ 5.0 GeV/c (dotted). Dashed: The corresponding differential cross section for the "Fermi" phase shift function, with parameters corresponding to Eq. (15.4).

Downloaded from https://www.cambridge.org/core. UNIVERSIDAD AUTONOMA METROPOLITANA, on 16 Nov 2026 at 02:58:46, subject to the Cambridge Core terms of use , available at https://www.cambridge.org/core/terms. https://doi.org/10.1017/9781316219256.019

15.2 "Fermi" and Square Root of "Fermi" Functions

We next consider another function with two sets of singularities, but where the second set of singularities now is of a lower degree compared to those of the "Fermi" function:

$$X(b_x) = \frac{A_{\mathrm{F}1}}{1+\exp[(b_x-c_1)/\beta_1]} + \frac{A_{\mathrm{F}2}}{\sqrt{1+\exp[(b_x-c_2)/\beta_2]}}, \quad \mathrm{Re}\, b_x > 0,$$
$$X(-b_x) = X(b_x), \tag{15.7}$$

i.e., a "Fermi" function plus the square root of one. Of course, the square root is subject to a sign ambiguity. We choose the sign for which the square root is positive along the real b_x-axis.

Again, it is instructive to first understand scattering from the square root function, i.e., the case $A_{\mathrm{F}1} = 0$. For the case of a pure real and repulsive ($A_{\mathrm{F}2}$ real and positive) square root function, the stationary points will be located on the real, negative b_x-axis. For moderate values of the momentum transfer, there will be two such points, eventually meeting at a rainbow point, beyond which one of them moves up into the second quadrant of the complex b_x-plane and becomes irrelevant, whereas the other moves down into the third quadrant. In addition, there will be a second branch (β) in the fourth quadrant, at $\mathrm{Re}\, b_x < c_2$. Below the rainbow point, it has $\mathrm{Im}\, b_x = -\pi\beta_2$.

While the square root is somewhat unfamiliar in this context, we note that the phase shift function is well-behaved at large real values of $\boldsymbol{b}$. It has in fact an exponential edge, but with a doubled surface thickness, namely $2\beta_2$.

In Fig. 15.7 we show the map of stationary points for the square root function. It has a rather unfamiliar feature, the trajectories of stationary points that emanate from the singularities at $(c_2, \beta_2) = (3, 0.5)$ fm do not continue out to $\mathrm{Re}\, b_x \to \pm\infty$. Instead, they extend *towards the central region*, namely the negative imaginary axis. This implies that the derivative $X'(b_x)$ can not become arbitrarily small along these trajectories. The smallest value, and hence the smallest value of the momentum transfer $\boldsymbol{q}$, for which we have a stationary point, is obtained for $\mathrm{Re}\, b_x \to 0$. When $\exp(-c_2/\beta_2) \ll 1$, this lowest value is given by

$$|\boldsymbol{q}|_{\min} \simeq \frac{|A_{\mathrm{F}2}|}{2\beta_2} e^{-c_2/\beta_2}. \tag{15.8}$$

For the parameters adopted in Fig. 15.7, the value is $|\boldsymbol{q}|_{\min} \simeq 5 \times 10^{-4}$ GeV.

The trajectories of stationary points are in this case, for $A_{\mathrm{F}2}$ purely imaginary, seen to approach the singularities at angles of $\pm\pi/3$, as opposed to $\pm\pi/4$ in the case of the ordinary "Fermi" phase shift function.

As discussed in Chapter 8, the finite value of $X'(b_x)$ for $\mathrm{Re}\, b_x \to 0$ implies that there is an evenness issue. The cusp at $b_x \to 0$ will at some critical momentum

Downloaded from https://www.cambridge.org/core. UNIVERSIDAD AUTONOMA METROPOLITANA, on 16 Nov 2026 at 02:58:46, subject to the Cambridge Core terms of use , available at https://www.cambridge.org/core/terms. https://doi.org/10.1017/9781316219256.019

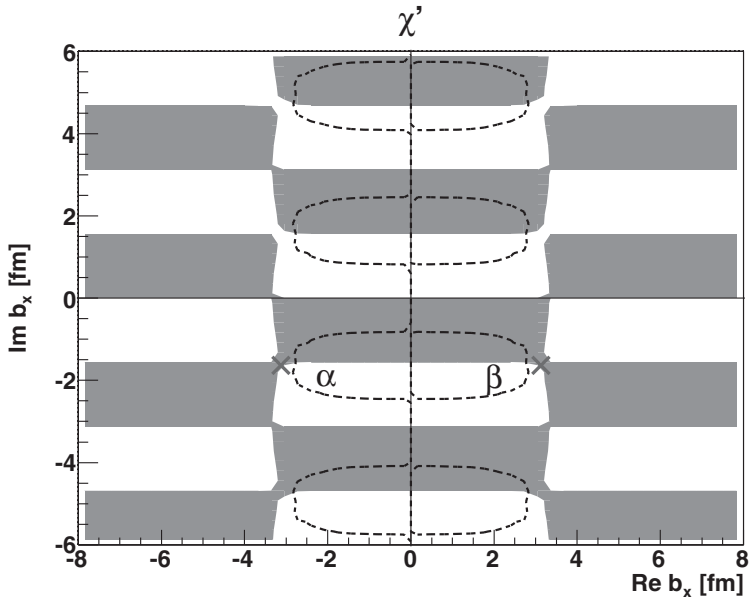


Figure 15.7 Regions of positive and negative values of $\mathrm{Re}\, X'(b_x)$, shown in the complex b_x-plane for the square root part of the phase shift function Eq. (15.7), with $A_{\mathrm{F}1} = 0$. The dashed curves indicate where $\mathrm{Im}\, X'(b_x) = 0$, i.e., where stationary points may be located. The crosses indicate singularities of the phase shift function. The shape parameters are $(c_2, \beta_2) = (3, 0.5)$ fm.

transfer lead to a differential cross section that ceases to fall exponentially. Different ways of making $X(b_x)$ even (or flat at the origin) will lead to slightly different differential cross sections, and will not be explored here. Instead, we focus on the asymptotic formulas.

The corresponding differential cross section is shown in Fig. 15.8 for the shape parameters Eq. (15.4), and $A_{\mathrm{F}2} = i$. Again, we compare with the ordinary "Fermi" phase shift function for the same shape parameters. For the square root function, the envelope of the differential cross section is seen to fall much more steeply, as expected because of the more diffuse surface.

Next, we consider the function Eq. (15.7) in full generality, with both $A_{\mathrm{F}1}$ and $A_{\mathrm{F}2}$ non-zero. Again, we will consider the more singular function, in this case the "Fermi" phase shift function, to have its singularities lower in the complex b_x-plane, i.e., we assume $\beta_1 > \beta_2$.

For the choice of parameters

$$\begin{aligned} A_{\mathrm{F}1} &= i, \qquad (c_1, \beta_1) = (2.7, 0.8)\ \mathrm{fm}, \\ A_{\mathrm{F}2} &= 0.5i, \quad (c_2, \beta_2) = (3, 0.5)\ \mathrm{fm}, \end{aligned} \tag{15.9}$$

we show in Fig. 15.9 the "map" of possible trajectories of stationary points in the complex b_x-plane. The relevant singularities are marked as crosses. The dashed

Downloaded from https://www.cambridge.org/core. UNIVERSIDAD AUTONOMA METROPOLITANA, on 16 Nov 2026 at 02:58:46, subject to the Cambridge Core terms of use, available at https://www.cambridge.org/core/terms. https://doi.org/10.1017/9781316219256.019

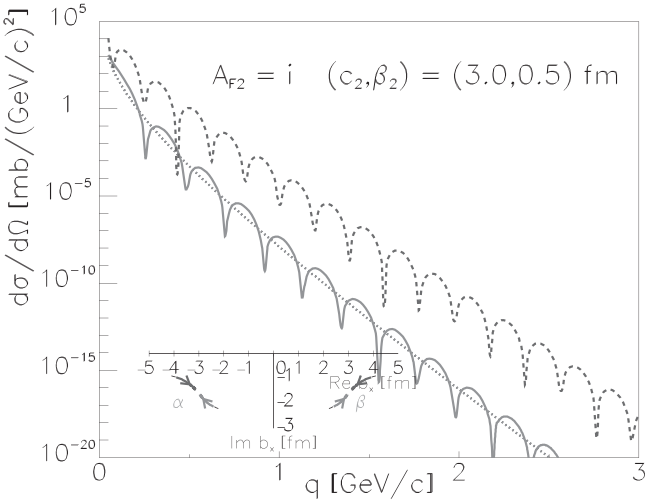


Figure 15.8 Solid: Differential cross sections corresponding to the phase shift function Eq. (15.7) for $A_{F1} = 0$, i.e., only the square root part is considered. The inserts show the trajectories of stationary points for $0.02\ \text{GeV/c} \le q \le 5.0\ \text{GeV/c}$ (dotted). Dashed: The corresponding differential cross section for the "Fermi" phase shift function, for the same parameters $(c, \beta) = (3, 0.5)$ fm.

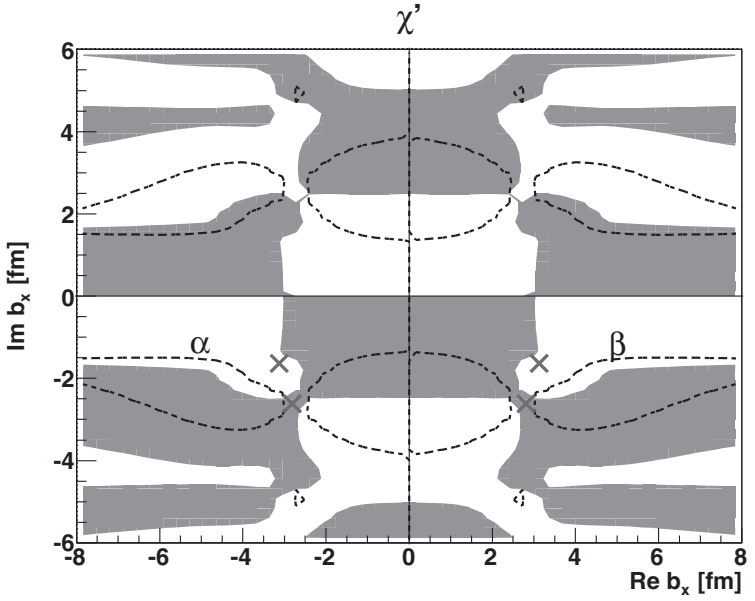


Figure 15.9 Similar to Fig. 15.7, for the phase shift function Eq. (15.7). The shape parameters are $A_{F1} = i$, $(c_1, \beta_1) = (2.7, 0.8)$ fm, and $A_{F2} = 0.5i$, $(c_2, \beta_2) = (3, 0.5)$ fm.

Downloaded from https://www.cambridge.org/core. UNIVERSIDAD AUTONOMA METROPOLITANA, on 16 Nov 2026 at 02:58:46, subject to the Cambridge Core terms of use , available at https://www.cambridge.org/core/terms. https://doi.org/10.1017/9781316219256.019

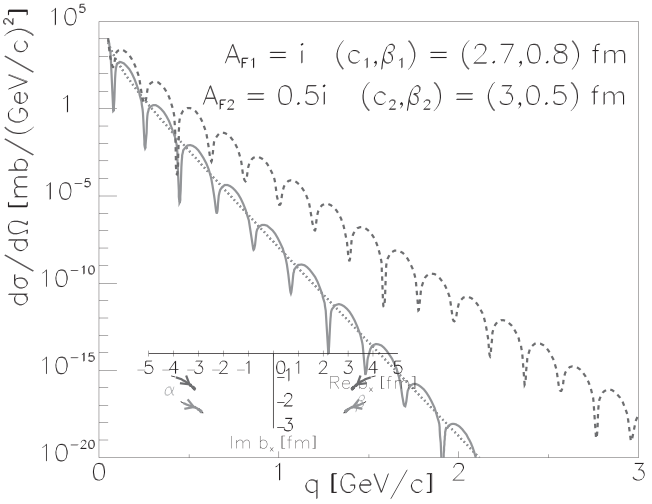


Figure 15.10 Solid: Differential cross sections corresponding to the phase shift function Eq. (15.7). The inserts show the trajectories of stationary points for 0.02 GeV/c $\leq q \leq$ 5.0 GeV/c (dotted). Dashed: The corresponding differential cross section for the "Fermi" phase shift function, for the parameters $(c_1, \beta_1) = (3, 0.5)$ fm.

lines labeled α and β are seen to stay in the white region (where $X'(b_x) > 0$) and circumvent the outer set of singularities by passing below, i.e., further away from the real axis.

The differential cross section corresponding to the parameters of Fig. 15.9 is shown in Fig. 15.10 (solid). For comparison, we also show the differential cross section corresponding to the simple "Fermi" phase function, with the parameters of Eq. (15.4) (dashed). While the two cross section patterns are quite different, what happens here is that the second term in Eq. (15.7) has very little effect. The slope and period of the cross section are basically determined by the first term, for which $(c_1, \beta_1) = (2.7, 0.8)$ fm.

Finally, let us consider a reduced strength of the "Fermi" function relative to its square root. For the choice of parameters

$$\begin{aligned} A_{\mathrm{F}1} &= 0.5i, \quad & (c_1, \beta_1) &= (3, 0.75) \text{ fm}, \\ A_{\mathrm{F}2} &= i, & (c_2, \beta_2) &= (2.5, 0.5) \text{ fm}, \end{aligned} \tag{15.10}$$

we show in Fig. 15.11 the corresponding "map" of stationary points. Here, the square root part plays almost no role, even though its strength is twice that of the ordinary "Fermi" phase shift function.

In Fig. 15.12 we have reduced the strength $A_{\mathrm{F}1}$ even further, $A_{\mathrm{F}1} = 0.2i$. At this point, the picture is quite similar to that for the pure square root function,

Downloaded from https://www.cambridge.org/core. UNIVERSIDAD AUTONOMA METROPOLITANA, on 16 Nov 2026 at 02:58:46, subject to the Cambridge Core terms of use , available at https://www.cambridge.org/core/terms. https://doi.org/10.1017/9781316219256.019

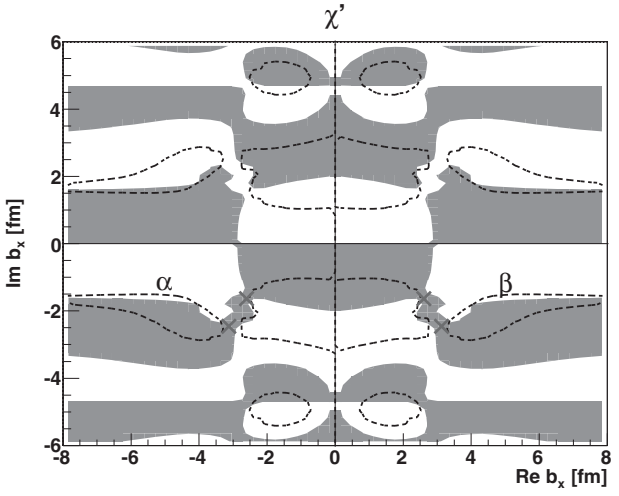


Figure 15.11 Similar to Fig. 15.9. The shape parameters are $A_{\mathrm{F}1} = 0.5i, (c_1, \beta_1) = (3, 0.75)$ fm, and $A_{\mathrm{F}2} = i$, $(c_2, \beta_2) = (2.5, 0.5)$ fm.

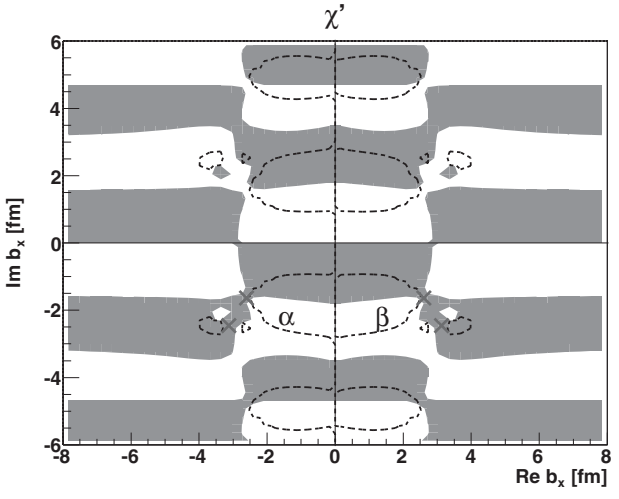


Figure 15.12 Similar to Fig. 15.11. The shape parameters are $A_{\mathrm{F}1} = 0.2i$, $(c_1, \beta_1) = (3, 0.75)$ fm, and $A_{\mathrm{F}2} = i$, $(c_2, \beta_2) = (2.5, 0.5)$ fm.

shown in Fig. 15.7. The ordinary "Fermi" phase shift function plays no significant role anymore.

Comparing the maps in Figs. 15.4 and 15.9 we note a qualitative difference. In Fig. 15.4 the trajectories of stationary points pass *above* (closer to the real axis) the outer singularities, whereas in Fig. 15.9 they pass *below* (further away from the real axis). This means that there must be a manifold of critical parameters. On one side

Downloaded from https://www.cambridge.org/core. UNIVERSIDAD AUTONOMA METROPOLITANA, on 16 Nov 2026 at 02:58:46, subject to the Cambridge Core terms of use , available at https://www.cambridge.org/core/terms. https://doi.org/10.1017/9781316219256.019

of this parameter manifold the trajectories of stationary points pass above the outer singularities, on the other side they pass below.

In the terminology of Eq. (15.2), assuming we keep $A_{F1}, c_1,$ and β_1 fixed, there is a critical value for A_{F2}, and/or c_2, and/or β_2 and/or the power p, for which the paths "jump" from one side of the singularities to the other. Such a "jump" will be accompanied by a dramatic change in the differential cross section pattern.

15.3 "Fermi" Plus Gaussian Functions

We shall next consider the composite phase shift function

$$X(b_x) = \frac{A_F}{1+\exp[(b_x-c)/\beta]} + A_G(b_x^2/\beta_G^2)^\nu \exp(-b_x^2/\beta_G^2), \qquad \mathrm{Re}\, b_x > 0,$$
$$X(-b_x) = X(b_x), \tag{15.11}$$

with $\nu = 0$, 1, or 2. We take, as a fixed reference,

$$A_F = i, \quad (c,\beta) = (3, 0.5)\ \text{fm}. \tag{15.12}$$

We start the discussion by showing in Fig. 15.13 the familiar "map" of $X'(b_x)$ for the case $A_G = i$, $\nu = 0$, and $\beta_G = 1.5$ fm. For simplicity, we take both functions to be purely imaginary (on the real axis), providing stationary points symmetrically

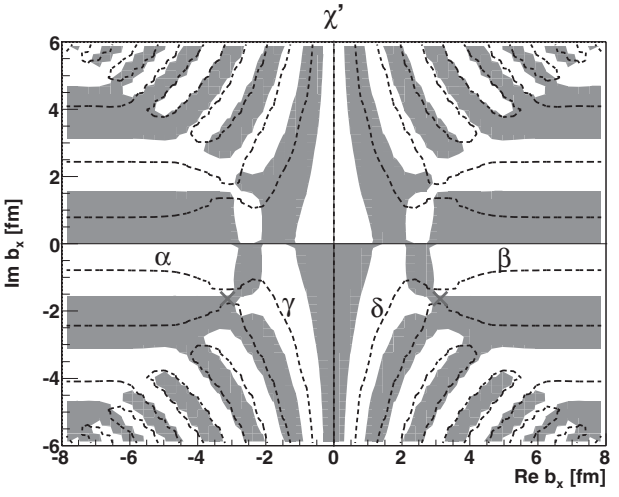


Figure 15.13 Regions of positive and negative values of $\mathrm{Re}\, X'(b_x)$, shown in the complex b_x-plane for the phase shift function Eq. (15.11). The dashed curves indicate where $\mathrm{Im}\, X'(b_x) = 0$, i.e., where stationary points may be located. The parameters of the "Fermi" function are given by Eq. (15.12), whereas those of the Gaussian are $A_G = i$, $\nu = 0$, and $\beta_G = 1.5$ fm. The crosses indicate singularities of the "Fermi" function.

Downloaded from https://www.cambridge.org/core. UNIVERSIDAD AUTONOMA METROPOLITANA, on 16 Nov 2026 at 02:58:46, subject to the Cambridge Core terms of use, available at https://www.cambridge.org/core/terms. https://doi.org/10.1017/9781316219256.019

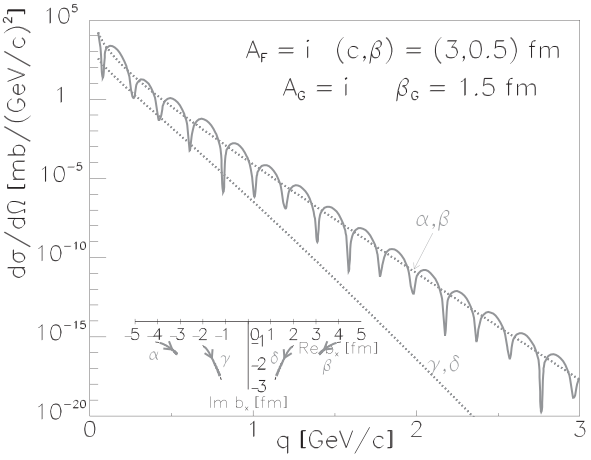


Figure 15.14 Differential cross sections corresponding to the phase shift function Eq. (15.11). The inserts show the trajectories of stationary points for $0.02\ \text{GeV/c} \leq q \leq 5.0\ \text{GeV/c}$ (dotted). The cross sections contributed by the individual stationary points are shown as dotted curves, labeled α, β and γ, δ.

located with respect to the imaginary axis. While the derivative of the "Fermi" function has second-order pole singularities in the complex plane, the Gaussian has essential singularities at $\pm i\infty$.

There are two relevant sets of stationary points. One set, (α, β), is associated primarily with the "Fermi" function, whereas the other (γ, δ) is associated primarily with the Gaussian. The essential singularity of the Gaussian will at large momentum transfers exert a strong influence on the stationary points.

The latter set is quite low in the complex plane, and thus contributes negligibly to the cross section, as shown in Fig. 15.14. It is clear that making the Gaussian more localized (smaller width β_G), the pair of stationary points (γ, δ) would be closer to the origin. This would have two effects:

i. The envelope of the amplitudes contributed by these stationary points would be less steep. At sufficiently large values of momentum transfer the scattering amplitudes contributed by these stationary points would thus become dominant.
ii. The resulting differential cross section would have a larger period of oscillations due to the smaller separation $\text{Re}\,(b_{\delta x} - b_{\gamma x})$.

As mentioned above, an interesting question is whether the trajectories α and β can connect to γ and δ. In order to explore this, we let $\nu > 0$ and also take a larger value of $|A_G|$. In Figs. 15.15 and 15.16 we show the corresponding "maps" for $\nu = 1$ and $\nu = 2$. In the case of $\nu = 1$ the extra factor $(b_x/\beta_G)^2$ has the effect of pushing the stationary points γ and δ somewhat further away from the origin and the negative imaginary axis. They are however not connected to α and β.

Downloaded from https://www.cambridge.org/core. UNIVERSIDAD AUTONOMA METROPOLITANA, on 16 Nov 2026 at 02:58:46, subject to the Cambridge Core terms of use, available at https://www.cambridge.org/core/terms. https://doi.org/10.1017/9781316219256.019

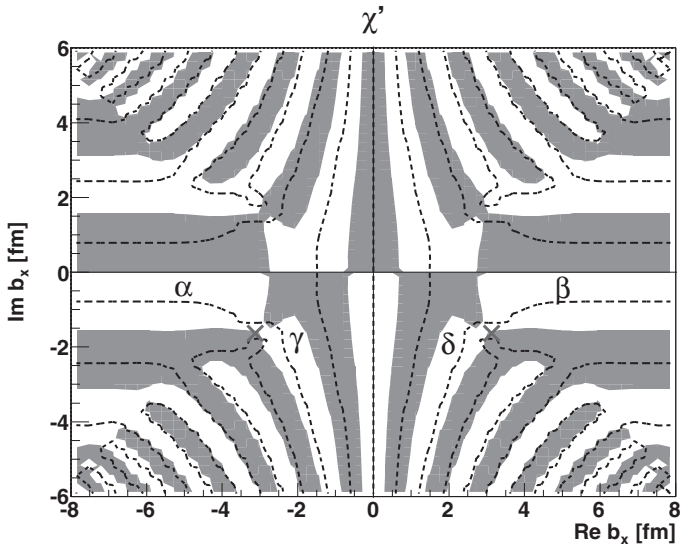


Figure 15.15 Similar to Fig. 15.13, except that for the Gaussian part $\nu = 1$.

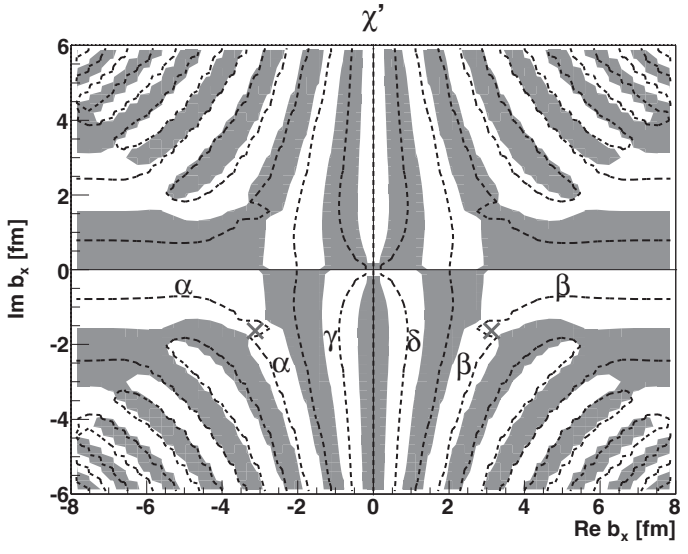


Figure 15.16 Similar to Fig. 15.13, except that for the Gaussian part $\nu = 2$.

With $\nu = 2$, on the other hand (see Fig. 15.16), the α and β trajectories continue down into the regions that were occupied by the γ and δ trajectories in the previous case, whereas a pair of "new" trajectories now appears closer to the imaginary axis. They are labeled γ and δ.

Downloaded from https://www.cambridge.org/core. UNIVERSIDAD AUTONOMA METROPOLITANA, on 16 Nov 2026 at 02:58:46, subject to the Cambridge Core terms of use , available at https://www.cambridge.org/core/terms. https://doi.org/10.1017/9781316219256.019

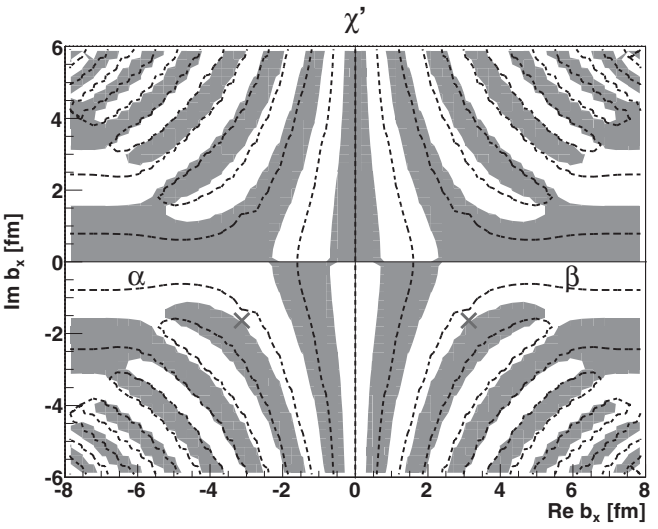


Figure 15.17 Similar to Fig. 15.15, except that $A_{\rm F} = 0.5i$ and for the Gaussian part we have $A_G = 10i$ and $\nu = 1$.

Another way to make the trajectories of stationary points α and β continue inwards towards the imaginary axis and down away from the real axis, is to increase the relative strength $|A_G|$ of the Gaussian function. This approach is illustrated in Fig. 15.17. With such a large weight on the Gaussian function, the stationary points α and β do not get "stuck" near the singularities of the "Fermi" function.

In this example, the trajectories pass on the inside of the singularities (shown as crosses in Fig. 15.17). If we instead increase the extension of the Gaussian from $\beta_G = 1.5$ fm to 3 fm, as illustrated in Fig. 15.18, the trajectories pass on the outside of the singularities, and they are also much more smooth. Of course, many intermediate situations can be imagined. If we reduce the strength of the Gaussian, stationary points will emerge near the singularities of the "Fermi" function. Eventually, as the strength of the Gaussian is further reduced, there will be two pairs of stationary points, as was the case in the initial example of Fig. 15.13 (for $A_{\rm F} = i$ and $\nu = 0$). Also, the relative magnitudes of the three shape parameters, c, β, and β_G, as well as the power ν, are important for the overall picture.

Such a smooth trajectory of stationary points going down into the complex plane, as shown in Fig. 15.18, can provide a lengthening of the period of the cross section oscillations, and a steepening of the envelope of these oscillations, as the momentum transfer increases. This is indeed the case, as shown in the corresponding differential cross section plot in Fig. 15.19. The envelope of the oscillation maxima is seen to bend down at large momentum transfers, together with some lengthening of the period.

Downloaded from https://www.cambridge.org/core. UNIVERSIDAD AUTONOMA METROPOLITANA, on 16 Nov 2026 at 02:58:46, subject to the Cambridge Core terms of use, available at https://www.cambridge.org/core/terms. https://doi.org/10.1017/9781316219256.019

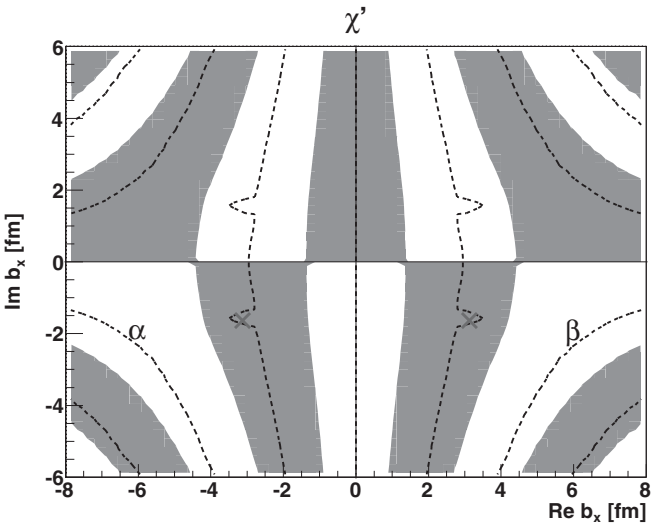


Figure 15.18 Similar to Fig. 15.17, except that for the Gaussian part we have $\beta_G = 3.0$ fm rather than 1.5 fm.

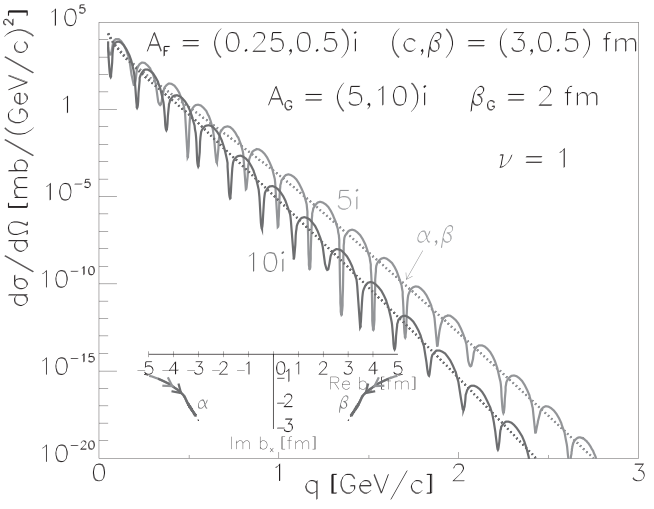


Figure 15.19 Differential cross sections corresponding to the phase shift function Eq. (15.11). The insert shows the trajectories of stationary points for $0.02\ \text{GeV/c} \leq q \leq 5.0\ \text{GeV/c}$ (dotted). The cross sections contributed by the individual stationary points are shown as dotted curves, labeled α, β.

In this figure we compare two cases, both having shape parameters $(c, \beta) = (3, 0.5)$ fm, $\beta_G = 2$ fm, and $\nu = 1$. They differ only in the strength parameters. The higher cross section curve refers to $A_F = 0.25i$ and $A_G = 5i$, while the lower cross section curve refers to $A_F = 0.5i$ and $A_G = 10i$. Since the shape parameters

Downloaded from https://www.cambridge.org/core. UNIVERSIDAD AUTONOMA METROPOLITANA, on 16 Nov 2026 at 02:58:46, subject to the Cambridge Core terms of use, available at https://www.cambridge.org/core/terms. https://doi.org/10.1017/9781316219256.019

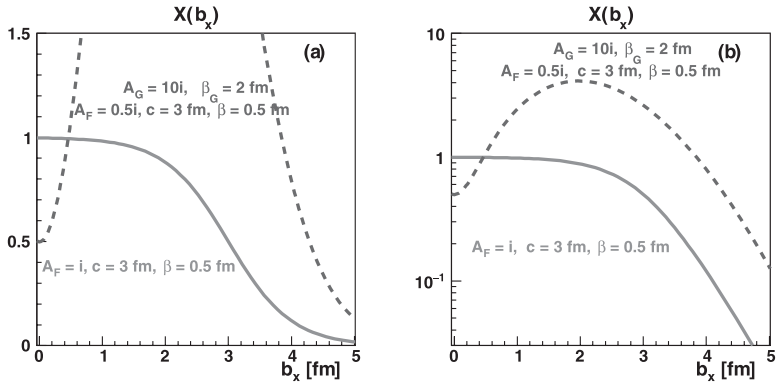


Figure 15.20 The phase shift function $X(b_x)$ of Eq. (15.11) for the parameters considered in Fig. 15.19 (dashed). For comparison, we also show the pure "Fermi" function (solid), for the parameters of Eq. 15.12. (a) linear representation; (b) logarithmic representation.

and the ratio A_{F}/A_G are the same in the two cases, it follows that their trajectories of stationary points are the same, as is seen from the inset. The different strength parameters lead however to different cross sections.

We have seen that for suitable parameters of the Gaussian function, the stationary points α and β continue to move inwards and down into the complex plane, without getting "stuck" at the pole singularities of the "Fermi" distribution. This leads to an interesting modification of the asymptotic behavior of the oscillations in the cross section, as compared with the stable pattern provided by the "Fermi" function.

It is a challenge to try to understand this in terms of the behavior of the phase shift function along the real axis. In Fig. 15.20 we show absolute values of phase shift functions, both in linear (a) and logarithmic (b) representations. Two cases are compared: (1) Pure "Fermi" function, i.e., $A_{\mathrm{G}} = 0$, and (2) $A_{\mathrm{G}} = 10i$ with $\nu = 1$ and $\beta_{\mathrm{G}} = 2$ fm, and a reduced "Fermi" strength, $A_{\mathrm{F}} = 0.5i$.

Attempting to understand the cross section behavior in terms of the values of the phase shift function along the real axis, two possible effects come to mind: (i) It could be due to the bulge just inside the surface region, or to (ii) a steeper behavior in the surface region. In terms of analytic functions, one can of course argue that the two aspects are related.

Downloaded from https://www.cambridge.org/core. UNIVERSIDAD AUTONOMA METROPOLITANA, on 16 Nov 2026 at 02:58:46, subject to the Cambridge Core terms of use , available at https://www.cambridge.org/core/terms. https://doi.org/10.1017/9781316219256.019